Optogenetic Control by Pulsed Illumination

Julia Hennemann,[a] Roman S. Iwasaki,[b] Tamara N. Grund,[a] Ralph P. Diensthuber,[b] Florian Richter,[b] and Andreas Möglich*[a, b]

[a] J. Hennemann, T. N. Grund, Prof. Dr. A. Möglich

Lehrstuhl für Biochemie, Universität Bayreuth, 95447 Bayreuth, Germany

[b] R. S. Iwasaki, Dr. R. P. Diensthuber, Dr. F. Richter, Prof. Dr. A. Möglich

Biophysikalische Chemie, Institut für Biologie, Humboldt-Universität zu Berlin, 10115 Berlin, Germany

*To whom correspondence should be addressed. Email: andreas.moeglich@uni-bayreuth.de; ORCID identifier: orcid.org/0000-0002-7382-2772

Abstract

Sensory photoreceptors evoke numerous adaptive responses in Nature and serve as light-gated actuators in optogenetics to enable the spatiotemporally precise, reversible and noninvasive control of cellular events. The output of optogenetic circuits can often be dialed in by varying illumination quality, quantity and duration. Here, we devise a programmable matrix of light-emitting diodes to efficiently probe the response of optogenetic systems to intermittently applied light of varying intensity and pulse frequency. Circuits for light-regulated gene expression markedly differed in their

responses to pulsed illumination of a single color which sufficed for sequentially triggering them. In addition to quantity and quality, the pulse frequency of intermittent light hence provides a further input variable for output control in optogenetics and photobiology. Pulsed illumination schemes allow the reduction of overall light dose and facilitate the multiplexing of several light-dependent actuators and reporters.

Keywords

light-oxygen-voltage; optogenetics; sensory photoreceptor; signal transduction; synthetic biology

Introduction

Sensory photoreceptors elicit a wide palette of light-dependent physiological responses in Nature,[1,2] e.g., plant development[3,4], phototaxis[5–7] and vision in diverse organisms[8]. They commonly feature modular architecture comprising photosensor (or, input) and effector (or, output) modules.[9] Photon absorption by the thermodynamically most stable, dark-adapted (or, resting) state D of the photosensor initiates a so-called photocycle, i.e. a series of photochemical events within and adjacent to the chromophore, leading to population of the light-adapted (or, signaling) state L.[9] In a process denoted dark recovery, the metastable light-adapted state L thermally reverts to the dark-adapted state D; in photochromic photoreceptors, secondary absorption of a photon can actively drive the reversion of L to D. In case of the light-oxygen-voltage (LOV) photoreceptors,[10,11] absorption of blue light by a flavin nucleotide chromophore in its quinone form leads to population of the excited singlet state S_1 that within nanoseconds undergoes intersystem crossing to the triplet state T_1. Within microseconds, the T_1 state decays to the signaling state L via formation of a covalent thioether bond between atoms C(4a) of the flavin isoalloxazine ring system and Sγ of a nearby conserved cysteine residue within the LOV photosensor. Concomitant with thioether formation, the N5 atom of the flavin chromophore is protonated which triggers hydrogen-bond rearrangements throughout the LOV photosensor. Studies on cysteine-devoid variants of LOV receptors revealed that N5 protonation is both necessary and sufficient for downstream signal propagation.[12] The stability of the thioether bond in cysteine-containing LOV receptors is strongly governed by temperature, solvent composition and molecular environment of the flavin chromophore.[13,14] Certain residue exchanges within the LOV photosensor adjacent to the flavin cofactor strongly stabilize or destabilize the thioether bond and thereby alter the lifetime of the signaling state L over up to several orders of magnitude. At least for LOV receptors, the deliberate variation of the dark-recovery kinetics via residue exchanges represents the means of choice for modulating effective light sensitivity at photostationary state under constant illumination.[9] By contrast, the absolute light sensitivity is determined by the absorption cross section and the quantum yield for formation of the signaling state which are largely invariant for a given photoreceptor class.

Sensory photoreceptors generally trigger biological reactions in response to incident light with exquisite spatiotemporal precision, non-invasiveness and full reversibility. These attractive attributes not only underpin numerous natural light-dependent processes, but also, they are central to the deployment of sensory photoreceptors in optogenetics.[15] Briefly, optogenetics denotes the (mostly) heterologous expression of sensory photoreceptors to render target cells, tissues and organisms light-sensitive and thus amenable to precise control in time and space by illumination. Initially developed in the neurosciences and exclusively reliant on light-gated ion channels and pumps,[6,7,16,17] optogenetics has been empowered by the advent of additional sensory photoreceptors and now affords light-

dependent control of numerous cellular parameters and processes.[9,18,19] In particular, the optogenetic repertoire has been greatly expanded by the engineering of novel sensory photoreceptors with custom-tailored light-dependent output. As a case in point, we constructed the blue-light-repressed histidine kinase YF1 by linking the LOV photosensor of the *Bacillus subtilis* YtvA protein,[20] engaged in mediating the general stress response in this bacterium,[21,22] to the effector module of the FixL histidine kinase from *Bradyrhizobium japonicum*.[23] Together with its cognate response regulator *Bj*FixJ, YF1 forms a light-regulated two-component system (TCS).[24] In its dark-adapted state D, YF1 readily phosphorylates *Bj*FixJ, thus triggering the transcription of target genes from a specific promoter, denoted FixK2. By contrast, in its light-adapted state L, YF1 acts as a net phosphatase that removes phosphoryl groups from phospho-*Bj*FixJ and consequently suspends target-gene expression. Based on the YF1/*Bj*FixJ TCS, the plasmids pDusk and pDawn allow light-repressed and light-enhanced gene expression, respectively, in *Escherichia coli* (Fig. 1A). The expression output of both pDusk and pDawn varies hyperbolically with the intensity of constant blue-light illumination.[25]

In optogenetics, a graded response of the system under study can often be effected via variation of the intensity and duration of constant illumination. Although this approach frequently suffices for adjusting the system response to desired set levels, we reasoned that additional optogenetic control could be exerted by resorting to pulsed illumination that is applied intermittently. This reasoning is supported by previous studies which used pulsed lighting schemes to control optogenetic circuits, e.g., references[26,27]. As mentioned above, even within a single photoreceptor class the dark-recovery kinetics can greatly vary. Put another way, photoreceptor variants can substantially differ in the refractory time after photoactivation during which they retain their signaling state L and have not fully returned to the dark-adapted state D. Accordingly, one should be able to differentially address and activate pairs of photoreceptors with pulsed illumination, provided they sufficiently differ in their recovery kinetics. To put this notion to the test, we have constructed a programmable matrix of light-emitting diodes (LEDs) that allows the parallel interrogation of numerous intensities and pulse frequencies of illumination. Using pDusk and pDawn as paradigms, we show that for certain lighting regimes the system response does not scale monotonically with the applied average light dose but is primarily governed by the pulse frequency of illumination. We exploit the differential response to pulsed, monochromatic illumination to sequentially control gene expression for pDawn variants that only differ in their dark-recovery kinetics. Taken together, our results show that the pulse frequency of intermittent light can serve as a further control variable, in addition to light quality (i.e. color) and quantity (i.e. intensity).

Results

Kinetic model for light-dependent gene expression.

To inform the experimental design for investigating pulsed illumination, we developed a kinetic framework for gene expression in the pDusk and pDawn systems that comprises three modules (Fig. 1B). The first module accounts for the photocycle of the YF1 photoreceptor. As determined by absorption spectroscopy, the rate constant k_{-1} for the monoexponential dark recovery of YF1 after prior photoactivation amounts to $(7.4 \pm 0.1)\cdot 10^{-4}$ s^{-1} at 37°C.[28] Experiments had previously demonstrated that the two LOV photosensors of the homodimeric YF1 receptor recover their dark-adapted state D independently from another with identical microscopic rate constants $k_R = k_{-1}/2$.[23] Likewise, light-induced formation of the signaling state L proceeds independently in the two LOV protomers. As the photochemical reactions leading to population of L are very fast in comparison to the timescales of dark recovery and gene expression, we lumped them together into a single unimolecular reaction with rate constant k_1, the magnitude of which depends on the intensity I of applied blue light according to $k_1 = k_I \cdot I$. The second module describes the phosphorylation and dephosphorylation of the response regulator *Bj*FixJ. As experimentally demonstrated,[23] YF1 is only active as a net histidine kinase provided both its LOV photosensors reside in their dark-adapted states which we denote as Y_{DD}. By contrast, if one or two LOV domains assume their light-adapted states, Y_{LD} and Y_{DL} or Y_{LL}, respectively, YF1 acts as a net phosphatase on phospho-*Bj*FixJ. As borne out by experiment,[23] the histidine kinase activity of YF1 hence recovers in sigmoidal rather than exponential fashion after prior photoactivation. The velocities of the *Bj*FixJ phosphorylation and dephosphorylation reactions catalyzed by YF1 are given by the rate constants k_K and k_P, respectively, and the spontaneous rate of hydrolysis of phospho-*Bj*FixJ is denoted k_H. The third module implements the expression from the FixK2 promoter. Phospho-*Bj*FixJ binds as a homodimer to this promoter with a dissociation constant of K_J to initiate transcription of a target gene with a rate constant of k_T. The kinetic model was expressed as a set of ordinary differential equations (cf. Experimental Section) and numerically solved (Fig. 1C). The model accurately recapitulated the experimental findings that the population of Y_{DD} decreases in exponential fashion during phases of blue-light illumination but recovers sigmoidally, i.e. with a lag phase, during dark periods. Because the phosphorylation degree of the response regulator *Bj*FixJ is governed by the relative concentrations of Y_{DD}, Y_{LD}, Y_{DL} and Y_{LL}, it also varies as a function of light over time.

In pDawn, target genes are expressed from the p_R promoter which is controlled by the phage λ repressor cI.[25] The expression of cI in turn occurs from the FixK2 promoter and is hence subject to light-dependent control by the YF1/*Bj*FixJ TCS. To evaluate experimental data obtained for the pDawn system, we expanded the above model accordingly (cf. Experimental Section).

Pulsed illumination for graded control of gene expression.

Next, we devised a setup for illuminating samples at defined light qualities, quantities and pulse frequencies (Fig. 1D, Suppl. Fig. 1). To this end, we constructed a programmable matrix of eight-by-eight three-color LEDs for the illumination from below of individual wells of 96-well microtiter plates. The setup employs open-source Arduino microcontrollers and commercially available electronics. A custom-made adapter piece and a mounting frame allow placement of the entire setup on a shaker platform. The light output of the LED matrix was calibrated with a lamp power meter. To facilitate the programming of the LED matrix, we developed a Python-based graphical user interface (cf. Suppl. Fig. 1). We note that our setup is similar to the light-plate apparatus (LPA) previously constructed by the Tabor laboratory.[29] In contrast to the LPA, our setup works with 96-well rather than 24-well plates, and its assembly does not require any soldering. On the downside, in our setup the LEDs are presently fixed to wavelengths of about 470, 525 and 620 nm, whereas the LPA can be variably outfitted with a range of different LEDs.

We employed the programmable LED matrix to systematically interrogate the response of the pDusk and pDawn systems to lighting regimes of different intensity and pulse frequency. To readily gauge the system output, we used a *Ds*Red Express2 fluorescence reporter gene.[30] *E. coli* cultures harboring pDusk-*Ds*Red or pDawn-*Ds*Red were incubated in black-wall, clear-bottom microtiter plates at 37°C for 16 h while being exposed to alternating cycles of darkness and blue-light illumination. While the illumination period was fixed at 30 s, the dark period ranged between 0 and 65 minutes. For different samples, the light intensity varied between 0 and 130 µW cm^{-2}. Following incubation, the *Ds*Red fluorescence and optical density at 600 nm (OD_{600}) were measured. Notably, the OD_{600} values of the cultures were independent of illumination indicating that phototoxicity did not significantly affect the experimental results. A contour plot of the results for the pDusk-*Ds*Red system shows that for a given light intensity reporter-gene output increased monotonically with the duration of the dark period (Fig. 2A); likewise, for a given dark period, the reporter output decreased monotonically with increasing light intensity. As expected,[25] the pDawn-*Ds*Red system exhibited inverted signal response with reporter-gene output monotonically decreasing with dark period but increasing with light intensity. Consistent with previous findings,[25] the maximum expression output for the pDawn-*Ds*Red system was around 3.6-fold times that for the pDusk-*Ds*Red system. To further characterize the system response of pDawn-*Ds*Red, we evaluated the expression output as a function of the applied light dose averaged over the entire experiment (Fig. 2B). Overall, the data can be described by a hyperbolic relation with a half-maximal light dose (LD_{50}) of 4.1 ± 0.8 µW cm^{-2}. For comparison, we previously obtained a value for LD_{50} of 12 ± 3 µW cm^{-2} for the pDawn-*Ds*Red system at constant illumination, albeit for quite different culture volumes and geometry of illumination.[25] Interestingly, at average light doses well below saturation, the system response did not scale monotonically with the overall

dose but rather depended on the pulse frequency of illumination (Fig. 2C). In particular, nearly identical overall input doses could result in quite different expression output as prominently seen in the dose regime 0-2.5 μW cm^{-2}. For example, a particularly pronounced differential effect was observed at an average light dose of around 0.6 μW cm^{-2}. Application of strong light pulses of 78 μW cm^{-2} every 65 minutes did not result in significant activation of gene expression, but when pulses of 8 μW cm^{-2} were applied every 6 minutes, gene expression was activated to around 40% of maximum extent. In general, for a given average dose, systematically higher gene expression output was obtained if light application was evenly distributed over several weaker pulses, rather than concentrated in a single strong pulse. Likewise, a desired expression output level could be obtained by different lighting schemes and overall light doses. For example, half-maximal activation of the pDawn-*Ds*Red system could either be achieved via continuous illumination at around 4 μW cm^{-2} (cf. above) or by applying light pulses of 30 s duration and 8 μW cm^{-2} intensity at 6-minutes intervals, corresponding to a 70% reduction of overall light dose. More generally, by using optimized illumination conditions, the applied light dose can hence be deliberately reduced to minimize detrimental phototoxic effects which to first approximation are expected to scale linearly with applied light dose. These findings also confirmed one of our initial premises, namely that in addition to light color and intensity, pulse frequency governs system output.

Sequential expression control using monochromatic light.

To assess whether the kinetic framework (cf. Fig. 1B) adequately accounts for the experimental results, we globally fitted the data for pDusk-*Ds*Red and pDawn-*Ds*Red to the numerical solution of the model (Fig. 2A). Altogether, the model well described the experimental data, and the fitted parameters assumed realistic values. For example, the YF1 kinase turnover (rate constant k_K) amounted to around 1.0 min^{-1} which compares to an experimental value of around 0.9 min^{-1} determined at 22°C.[23] Moreover, the YF1 phosphatase turnover was fitted as 15 min^{-1} which agrees with the experimental finding that dephosphorylation of *Bj*FixJ proceeds much faster than its phosphorylation. Having corroborated our kinetic model, we predicted how system output varies if the underlying YF1/*Bj*FixJ TCS is modified. Specifically, we reasoned that modulation of the dark-recovery kinetics k_R of YF1 via mutagenesis should strongly affect the system response to pulsed illumination. To this end, we exchanged in the YF1 receptor the residue valine at position 28 for either threonine (V28T) or isoleucine (V28I) because corresponding exchanges in the LOV2 domain of *Avena sativa* phototropin 1 had strongly accelerated and decelerated, respectively, dark-recovery kinetics.[31] The YF1 variants V28T and V28I were heterologously expressed, purified and their dark-recovery kinetics were monitored by absorption spectroscopy at 37°C (Fig. 3A). Whereas the rate constant of dark recovery for V28T of $k_{-1} = (1.7 \pm 0.1)\cdot10^{-3}$ s^{-1} was around twice as large as that for the original YF1, in case of V28I the recovery reaction was slowed down by around 10-fold relative to YF1 to $k_{-1} = (5.3 \pm 0.1)\cdot10^{-5}$ s^{-1}.

The residue exchanges V28T and V28I were also introduced into the pDusk-*Ds*Red and pDawn-*Ds*Red systems, and the gene expression output was monitored at different light intensities and pulse frequencies (Fig. 3B). Consistent with the altered dark-recovery kinetics, the variants V28T and V28I showed decreased and increased light sensitivity, respectively, in both the pDusk and pDawn contexts. In particular, the V28I variants were efficiently switched even at low light doses and extended dark periods. Inspection of the gene expression output for the YF1, V28T and V28I variants in the pDawn-*Ds*Red context revealed areas in the intensity/pulse frequency space where a subset of variants was efficiently switched while the other variants hardly responded. Based on these data, we reran the gene expression experiments for the pDawn-*Ds*Red variants YF1, V28T and V28I at five discrete intensity/pulse frequency settings. By choosing extended dark periods (20 min) and moderate blue-light intensities (12 μW cm^{-2}), the V28I variant of the system could be activated to around half-maximal extent without significantly activating either of the other two systems. At somewhat higher intensity (35 μW cm^{-2}) and shorter dark period (6 min), the original YF1 system could be more strongly activated than the V28T variant. In regimes of high light intensity (constant illumination at 65 μW cm^{-2}), all three variants were activated to similar extent. Notably, the use of pulsed illumination was required for individual activation of the systems, whereas constant illumination (i.e. a dark period of 0 in Fig. 3B) did not suffice for discriminating between the different systems. Evidently, pulsed illumination affords enhanced control, for example to enable the parallel use of several photoreceptor systems and their consecutive activation with monochromatic light.

Response of derivative gene expression systems to pulsed illumination.

Using the programmable LED matrix, we also interrogated the intensity/pulse frequency response of derivative pDusk and pDawn systems that harbor YF1 variants with altered functional properties (Fig. 4). The single residue exchanges D21V and H22P, both situated at the dimer interface of homodimeric YF1, have been shown to invert the response to light.[32,33] We introduced these mutations into the pDusk-*Ds*Red and pDawn-*Ds*Red contexts and measured gene expression output as a function of intensity and pulse frequency of illumination. In the pDusk-*Ds*Red setting, both the D21V and H22P variants showed the inverted response to illumination relative to YF1 in that reporter output decreased with increasing dark period and increased with light intensity. Whereas reporter-gene expression in the H22P variant was upregulated by up to 14-fold, in the D21V variant a maximum upregulation of only 6-fold was achieved. For reference, in the original pDusk-*Ds*Red light induced a downregulation of reporter-gene expression by up to 11-fold. Within the pDawn-*Ds*Red context, both the D21V and the H22P variant also displayed inverted behavior relative to the original YF1 with reporter-gene expression that increased with dark period and decreased with light intensity. Again, the maximum degree of light regulation for D21V was less pronounced than that obtained for H22P.

Next, we assessed the response to intensity and pulse frequency of illumination in pDusk and pDawn systems harboring YF1 variants that lack the conserved adduct-forming cysteine residue, number 62, inside the LOV photosensor (Fig. 4 and Suppl. Fig. 2). We previously showed that such cysteine-devoid LOV receptors can still retain light sensitivity and downstream signal transduction because, in the absence of the conserved cysteine, blue-light absorption promotes reduction of the flavin chromophore to the neutral semiquinone state (NSQ).[12] Notably, formation of the NSQ entails protonation of the flavin N5 atom which is key to triggering downstream responses. Introduction of the C62A substitution substantially impaired the regulation of reporter-gene expression in both the pDusk-*Ds*Red and pDawn-*Ds*Red contexts relative to the original YF1-based variants, in agreement with previous observations.[12] Although the difference between minimum and maximum reporter expression was attenuated due to cysteine removal, the sensitivity to light of different pulse frequencies and intensities stayed largely invariant. These data indicate that inside bacterial cells the cysteine-devoid variants possess similar kinetics for formation and depletion of the signaling state as the cysteine-containing variants. We also introduced the C62A substitution in the background of the signal-inverted D21V and H22P variants. In the pDusk-*Ds*Red context, light responsiveness was retained for both D21V:C62A and H22P:C62A. Remarkably, although pDusk-*Ds*Red H22P:C62A suffered a slight reduction in light sensitivity compared to the H22P variant, it displayed essentially the same maximum degree of regulation. In the pDawn-*Ds*Red context, regulation by light was largely abolished for the D21V:C62A variant whereas the H22P:C62A variant retained light responsiveness albeit to lesser extent than the H22P variant.

Discussion

Genetically encoded, light-gated circuits enable the control and analysis of cellular processes and parameters with unprecedented spatiotemporal accuracy, reversibility and noninvasiveness. A cohort of natural and engineered sensory photoreceptors underpin a multitude of optogenetic applications in many areas of basic and applied science, including biotechnology, synthetic biology and cell biology.[9,18] Of particular benefit, the output of optogenetic circuits can often be adjusted in graded manner by altering the quality (color), quantity (intensity) and duration of illumination. Here, we have explored the use of pulsed illumination schemes for enhanced optogenetic control. Employing as paradigms setups for light-regulated gene expression in prokaryotes,[25] we demonstrate that variation of the pulse frequency of illumination provides an additional input variable for controlling the output of light-gated systems. Specifically, we exploit that sensory photoreceptors retain their signaling state for a refractory time after illumination ceases before eventually resuming their dark-adapted resting state. As a consequence, the physiological effect induced by light persists for a period whose length is

strongly governed by the dark-recovery kinetics of the underlying photoreceptor. In addition, processes downstream of the actual photoreceptor may also persist and hence contribute to the overall dark-recovery kinetics of the entire system under study. By analyzing the response function of a given optogenetic circuit to varying intensities and pulse frequencies of light, optimized illumination protocols may be devised that maximize the biological effect but minimize the overall light dose and detrimental phototoxic processes. Although the precise outcome will differ between scenarios, we expect the maximum effect for pulse frequencies on the timescale of the recovery kinetics of the system under study. We note that pulsed illumination also provides an avenue towards temporally synchronizing optogenetic circuits, e.g., across a cell culture population.[34] Moreover, pulsed illumination is suitable for separately addressing pairs of photoreceptors even if they respond to the same light quality (cf. Fig. 3). In particular for LOV and rhodopsin photoreceptors,[8,14] and to lesser extent also for cryptochrome photoreceptors,[35] molecular determinants that govern the dark recovery process have been identified. The kinetics of dark recovery can often be deliberately modulated over a wide range by substitution of certain protein residues near the chromophore. In this manner, the response of the photoreceptor to pulsed illumination can thus be adjusted as demanded by a given application. The ability to differentially control several photoreceptor systems with a single light color can reduce the required number of independent input channels which particularly benefits experiments in which photoreceptor systems are multiplexed and/or are combined with fluorescent proteins. Evidently, pulsed illumination schemes extend to more than one light color, which is of especial utility for bimodally switchable, photochromic photoreceptors.[9,36]

To unravel the response of optogenetic circuits to pulsed light in facile manner, we have developed a versatile programmable LED matrix for the parallel illumination of individual wells of microtiter plates at varying intensity and pulse frequency. We deployed this setup to characterize the response of the pDusk and pDawn systems for light-regulated gene expression in prokaryotes.[25] Introduction of the residue exchanges V28T or V28I in YF1 sped up or down, respectively, the recovery kinetics of both the pDusk and pDawn systems, and accordingly decreased or increased, respectively, their effective light sensitivities (cf. Fig. 3A, B). Judiciously chosen pulsed illumination enabled the differential optogenetic control of gene expression for pDawn variants, even with a single light color (cf. Fig. 3C). The LED matrix also served to analyze in more detail the response to illumination of pDusk and pDawn variants in which the YF1 photoreceptor lacks the conserved, active-site cysteine residue.[12] At least in some variants, essentially intact light response was retained even after removal of this cysteine (cf. Fig. 4 and Suppl. Fig. 2). In the absence of the cysteine residue, blue light promotes reduction of the flavin chromophore to the neutral semiquinone (NSQ) radical state, which owing to its protonation at the N5 atom, can still elicit downstream signaling processes.[12] The present data show that at physiological

conditions this process can be as efficient as signal transduction by the original cysteine-containing LOV receptors.

In general, the programmable LED matrix and related devices for automated illumination,[29,37–41] stand to facilitate the analysis and application of optogenetic circuits and other light-responsive systems. These lighting setups directly pertain to the optogenetic regulation of gene expression in prokaryotes[25,39,42–49] and eukaryotes,[36,50–52] and readily extend to additional optogenetic experiments.[53,27,54] More generally, setups for programmable, parallelized illumination may also benefit the analysis of other light-sensitive biological and chemical processes, for example the cultivation of photoautotrophic organisms like cyanobacteria.[55]

Experimental Section

Assembly of the programmable LED matrix.

To examine in facile manner light-dependent biological processes at varying intensities and pulse frequencies of illumination, we constructed a programmable matrix of light-emitting diodes (LEDs). A commercially available circuit board with an eight-by-eight array of three-color LEDs (Adafruit NeoPixel, Adafruit industries, New York, USA) was outfitted with a custom-made adapter upon which a standard 96-well microtiter plate (MTP) can be placed (cf. Fig. 1D and Suppl. Fig. 1). The adapter thus enables the illumination of 64 individual wells of an MTP from below. To achieve optical isolation between adjacent wells, the adapter features recessed holes into which the individual LEDs are embedded. In addition, MTPs with transparent bottom and black walls were used (Greiner BioOne, Frickenhausen, Germany). The entire assembly was encased in a mounting frame to allow placement on a standard MTP shaker (Suppl. Fig. 1). While these parts were originally shaped by subtractive manufacturing, we also supply templates for additive manufacturing, i.e. 3D printing (available for download at http://www.moeglich.uni-bayreuth.de/en/software). A programmable Arduino Uno microcontroller was used to set the color, intensity and pulse frequency of illumination for the individual pixels of the LED matrix (part list and circuit layout available from the above URL). Each LED pixel comprises three color channels (470, 525 and 620 nm, respectively) which can be controlled via pulse-width modulation in 256 brightness steps (8 bit). We developed a Python-based graphical user interface to facilitate the configuration of the LED matrix (Suppl. Fig. 1; also available at the above URL). As output, the user interface generates an Arduino sketch file to be uploaded to the Arduino microcontroller. To improve the temporal accuracy of the Arduino microcontroller, optionally a real-time clock (RTC DS3221 Precision, Adafruit industries, New York, USA) can be implemented. Actual light intensities for each LED matrix were calibrated with a power meter (model 842-PE, Newport, Darmstadt, Germany) and a silicon photodetector (model 918D-UV-OD3, Newport).

Light-dependent gene expression at varying intensity and pulse frequency of illumination.

Variants of YF1 were generated by site-directed mutagenesis in the background of the reporter plasmids pDusk-*Ds*Red and pDawn-*Ds*Red according to the QuickChange protocol (Invitrogen, Life Technologies).[25] The identity of all constructs was confirmed by DNA sequencing (GATC Biotech). All experiments were carried out in the *E. coli* CmpX13 strain in Luria-Bertani (LB) medium plus 50 µg mL^{-1} kanamycin.[56] To determine the dependence of gene expression on varying lighting schemes, 5-mL starter cultures were inoculated from freshly transformed plates and were grown at 37°C to an optical density at 600 nm (OD_{600}) of 0.3 under non-inducing conditions (i.e. in the dark for pDawn-*Ds*Red or at 100 µW cm^{-2} 470-nm light for pDusk-*Ds*Red constructs). 10 µL of these cultures were used to inoculate 15 mL LB medium, and 200 µL each of this solution were added to 64 wells of a black-wall, transparent-bottom 96-well microtiter plate (Greiner BioOne, Frickenhausen, Germany). The MTP plate was sealed with gas-permeable sealing film BF-400-S (Corning, New York, USA) and placed on top of the LED-array setup. The assembly was mounted on an MTP shaker (PMS-1000i Microplate Shaker, Grant Instruments, Cambridge, UK) and incubated at 37 °C and 600 rpm for 16 h (HN-2 Herp Nursery II, Lucky Reptile, Waldkirch, Germany). Dark conditions were achieved by covering the windows of the incubator and all displays with black plastic foil. During incubation, each well was repeatedly illuminated by light of 470 ± 5 nm, where intensity varied between 0-130 µW cm^{-2}. Pulses of blue light for 30 seconds were followed by dark periods of between 0 and 65 minutes. Following incubation, OD_{600} and *Ds*Red fluorescence were measured for each well in a Tecan Infinite M200 PRO plate reader (Tecan Group Ltd., Männedorf, Switzerland) using excitation and emission wavelengths of 554 ± 9 nm and 591 ± 20 nm, respectively. Fluorescence data were normalized to OD_{600} and represent the averages of three biological replicates ± s.d.

Kinetic model for light-dependent gene expression.

Experimental data were represented as contour plots as a function of the duration of the dark interval and intensity of pulsed illumination. To quantitatively evaluate the experimental data for pDusk-*Ds*Red, the kinetic model shown in Fig. 1B was cast as a set of ordinary differential equations (ODEs):

$$d[Y_{DD}]/dt = -2 \cdot k_I \cdot I \cdot [Y_{DD}] + k_R \cdot ([Y_{LD}] + [Y_{DL}]) \quad (1)$$

$$d[Y_{LD}]/dt = -(k_R + k_I \cdot I) \cdot [Y_{LD}] + k_I \cdot I \cdot [Y_{DD}] + k_R \cdot [Y_{LL}] \quad (2)$$

$$d[Y_{DL}]/dt = -(k_R + k_I \cdot I) \cdot [Y_{DL}] + k_I \cdot I \cdot [Y_{DD}] + k_R \cdot [Y_{LL}] \quad (3)$$

$$d[Y_{LL}]/dt = -2 \cdot k_R \cdot [Y_{LL}] + k_I \cdot I \cdot ([Y_{LD}] + [Y_{DL}]) \quad (4)$$

$$d[J]/dt = -k_K \cdot [Y_{DD}] \cdot [J] + k_H \cdot [J_P] + k_P \cdot ([Y_{LD}] + [Y_{DL}] + [Y_{LL}]) \cdot [J_P] \quad (5)$$

$$d[J_P]/dt = k_K \cdot [Y_{DD}] \cdot [J] - k_H \cdot [J_P] - k_P \cdot ([Y_{LD}] + [Y_{DL}] + [Y_{LL}]) \cdot [J_P] \quad (6)$$

$$d[R]/dt = k_T \cdot [J_P]^2 / \left(K_J + [J_P]^2\right) \quad (7)$$

In eqs. (1-7), [Y_{DD}], [Y_{LD}], [Y_{DL}] and [Y_{LL}] denote the concentrations of YF1 with its two LOV photosensors in the states indicated by the subscripts (i.e. D, dark-adapted, and L, light-adapted); [J] and [J_P] denote the concentrations of the response regulator *Bj*FixJ in dephosphorylated and phosphorylated states, respectively; and [R] denotes the concentration of *Ds*Red reporter protein. The microscopic rate constants $k_I \cdot I$ and k_R describe photoactivation and dark recovery processes of the LOV photosensors, where I is the applied light intensity; k_K and k_P denote the rate constants for phosphorylation and dephosphorylation of *Bj*FixJ; K_J is the dissociation constant for binding of phospho-*Bj*FixJ to the FixK2 promoter; and k_T is the rate transcription from said promoter upon activation by phospho-*Bj*FixJ. For the evaluation of pDawn, eq. (7) was replaced by eqs. (8-9):

$$d[\lambda]/dt = k_T \cdot [J_P]^2 / \left(K_J + [J_P]^2\right) - k_D \cdot [\lambda] \quad (8)$$

$$d[R]/dt = k_\lambda \cdot K_\lambda / (K_\lambda + [\lambda]^4) \quad (9)$$

In eqs. (8-9), [λ] denotes the concentration of the phage λ cI repressor that forms part of the pDawn system; K_λ and k_λ, respectively, are the dissociation constant of λ cI to the pR promoter and the basal transcription rate from this promoter; k_D denotes the rate constant for degradation of λ cI which had been destabilized by appendage of a C-terminal LVA tag.[25] We note that these models are but approximations of the experimental systems under study. For example, growth and dilution of the culture are not taken into account.

Using Python, the experimental data for the pDusk and pDawn systems were globally fitted to the numerical solution of the ODE system defined in eqs. (1-9). During periods of darkness, the intensity I and hence the rate constant $k_1 = k_I \cdot I$ were set to zero. To reduce the number of floating parameters and achieve a better fit convergence, several parameters were held constant. Specifically, the rate constant for the dark recovery of YF1 at 37°C, k_R, was fixed at the value of $3.7 \cdot 10^{-4}$ s^{-1} as experimentally determined by absorption spectroscopy. The rate constant for spontaneous hydrolysis of phospho-*Bj*FixJ k_H was fixed at a low value of 1 h^{-1}; the rate constants for transcription from the FixK2 and pR promoters were arbitrarily restrained at 1 s^{-1}. The remaining parameters were fitted as $k_I = 1.2 \cdot 10^{-4}$ (μW cm^{-2})$^{-1}$ min^{-1}, $k_K = 1.0$ min^{-1}, $k_P = 15$ min^{-1}, $K_J = 35$, $k_D = 2$ min^{-1}, and $K_\lambda = 0.02$.

Protein expression and purification.

Variants of YF1 were generated by site-directed mutagenesis in the background of the expression plasmid pET-41a-YF1 via the QuikChange protocol (Invitrogen, Life Technologies GmbH). Purification of YF1 and its variants V28I and V28T was carried out as described previously.[32] Briefly, expression in *E. coli* CmpX13 cells was induced by adding 1 mM isopropyl β-D-1-thiogalactopyranoside, and cells were then incubated for 4 h at 37°C. Cells were harvested by centrifugation and lysed by ultrasound. Proteins were purified by Ni:NTA affinity chromatography and dialyzed into storage buffer (10 mM Tris/HCl pH 8.0, 10 mM NaCl, 10% (w/v) glycerol). Protein concentration was determined by absorption measurements with an Agilent 8453 UV–vis spectrophotometer (Agilent Technologies, Santa Clara, USA) using an extinction coefficient at 450 nm of 12,500 M^{-1} cm^{-1}.

Spectroscopic analysis.

Absorption spectra of YF1 and its variants V28T and V28I were collected on an Agilent 8453 diode-array spectrophotometer as a function of time at a controlled temperature of 37°C. To photoactivate the samples, they were illuminated for 10 s with an LED (450 nm, 30 mW cm^{-2}), and dark recovery was followed by continuously recording absorption spectra. Spectra were corrected for baseline drift by subtracting the absorbance reading at 600 nm. Time-dependent absorption at 450 nm was fitted to a single-exponential function to determine the rate constant k_{-1} for the dark recovery.

Acknowledgements

Discussions with Drs. Philipp Sasse (University of Bonn), Harald Janovjak (EMBL Australia) and members of the Möglich lab are greatly appreciated. Financial support through a Sofja-Kovalevskaya Award by the Alexander-von-Humboldt Foundation and project MO2192/3-1 by the Deutsche Forschungsgemeinschaft are gratefully acknowledged.

References

[1] P. Hegemann, *Annu. Rev. Plant Biol.* **2008**, *59*, 167–189.
[2] A. Möglich, X. Yang, R. A. Ayers, K. Moffat, *Annu. Rev. Plant Biol.* **2010**, *61*, 21–47.
[3] J. Hughes, *Annu. Rev. Plant Biol.* **2013**, *64*, 377–402.
[4] J. M. Christie, L. Blackwood, J. Petersen, S. Sullivan, *Plant Cell Physiol.* **2015**, *56*, 401–413.
[5] T. W. Engelmann, *Pflüger, Arch. für die Gesammte Physiol. des Menschen und der Thiere* **1883**, *30*, 95–124.
[6] G. Nagel, D. Ollig, M. Fuhrmann, S. Kateriya, A. M. Musti, E. Bamberg, P. Hegemann, *Science* **2002**, *296*, 2395–2398.
[7] G. Nagel, T. Szellas, W. Huhn, S. Kateriya, N. Adeishvili, P. Berthold, D. Ollig, P. Hegemann, E.

Bamberg, *Proc. Natl. Acad. Sci. U. S. A.* **2003**, *100*, 13940–13945.
[8] O. P. Ernst, D. T. Lodowski, M. Elstner, P. Hegemann, L. S. Brown, H. Kandori, *Chem. Rev.* **2014**, *114*, 126–163.
[9] T. Ziegler, A. Möglich, *Front. Mol. Biosci.* **2015**, *2*, 30.
[10] J. M. Christie, P. Reymond, G. K. Powell, P. Bernasconi, A. A. Raibekas, E. Liscum, W. R. Briggs, *Science (80-.).* **1998**, *282*, 1698–1701.
[11] K. S. Conrad, C. C. Manahan, B. R. Crane, *Nat. Chem. Biol.* **2014**, *10*, 801–809.
[12] E. F. Yee, R. P. Diensthuber, A. T. Vaidya, P. P. Borbat, C. Engelhard, J. H. Freed, R. Bittl, A. Möglich, B. R. Crane, *Nat. Commun.* **2015**, *6*, 10079.
[13] M. T. Alexandre, J. C. Arents, R. van Grondelle, K. J. Hellingwerf, J. T. Kennis, *Biochemistry* **2007**, *46*, 3129–3137.
[14] A. Pudasaini, K. K. El-Arab, B. D. Zoltowski, *Front. Mol. Biosci.* **2015**, *2*, 18.
[15] K. Deisseroth, *Nat Methods* **2011**, *8*, 26–29.
[16] E. S. Boyden, F. Zhang, E. Bamberg, G. Nagel, K. Deisseroth, *Nat. Neurosci.* **2005**, *8*, 1263–1268.
[17] F. Zhang, L.-P. Wang, M. Brauner, J. F. Liewald, K. Kay, N. Watzke, P. G. Wood, E. Bamberg, G. Nagel, A. Gottschalk, et al., *Nature* **2007**, *446*, 633–639.
[18] N. A. Repina, A. Rosenbloom, A. Mukherjee, D. V. Schaffer, R. S. Kane, *Annu. Rev. Chem. Biomol. Eng.* **2017**, *8*, 13–39.
[19] Q. Liu, C. L. Tucker, *Curr. Opin. Chem. Biol.* **2017**, *40*, 17–23.
[20] A. Losi, E. Polverini, B. Quest, W. Gärtner, *Biophys. J.* **2002**, *82*, 2627–2634.
[21] S. Akbar, T. A. Gaidenko, C. M. Kang, M. O'Reilly, K. M. Devine, C. W. Price, *J Bacteriol* **2001**, *183*, 1329–38.
[22] M. Avila-Perez, K. J. Hellingwerf, R. Kort, *J Bacteriol* **2006**, *188*, 6411–4.
[23] A. Möglich, R. A. Ayers, K. Moffat, *J. Mol. Biol.* **2009**, *385*, 1433–1444.
[24] E. J. Capra, M. T. Laub, *Annu. Rev. Microbiol.* **2012**, *66*, 325–347.
[25] R. Ohlendorf, R. R. Vidavski, A. Eldar, K. Moffat, A. Möglich, *J. Mol. Biol.* **2012**, *416*, 534–542.
[26] L. J. Bugaj, A. T. Choksi, C. K. Mesuda, R. S. Kane, D. V Schaffer, *Nat. Methods* **2013**, *10*, 249–252.
[27] J. E. Toettcher, O. D. Weiner, W. A. Lim, *Cell* **2013**, *155*, 1422–1434.
[28] R. P. Diensthuber, C. Engelhard, N. Lemke, T. Gleichmann, R. Ohlendorf, R. Bittl, A. Möglich, *ACS Synth. Biol.* **2014**, *3*, 811–819.
[29] K. P. Gerhardt, E. J. Olson, S. M. Castillo-Hair, L. A. Hartsough, B. P. Landry, F. Ekness, R. Yokoo, E. J. Gomez, P. Ramakrishnan, J. Suh, et al., *Sci Rep* **2016**, *6*, 35363.
[30] R. L. Strack, D. E. Strongin, D. Bhattacharyya, W. Tao, A. Berman, H. E. Broxmeyer, R. J. Keenan, B. S. Glick, *Nat. Methods* **2008**, *5*, 955–957.
[31] F. Kawano, Y. Aono, H. Suzuki, M. Sato, *PLoS One* **2013**, *8*, e82693.
[32] R. P. Diensthuber, M. Bommer, T. Gleichmann, A. Möglich, *Structure* **2013**, *21*, 1127–1136.
[33] T. Gleichmann, R. P. Diensthuber, A. Möglich, *J. Biol. Chem.* **2013**, *288*, 29345–29355.
[34] H. E. Johnson, Y. Goyal, N. L. Pannucci, T. Schüpbach, S. Y. Shvartsman, J. E. Toettcher, *Dev. Cell* **2017**, *40*, 185–192.
[35] A. Taslimi, B. Zoltowski, J. G. Miranda, G. P. Pathak, R. M. Hughes, C. L. Tucker, *Nat. Chem. Biol.* **2016**, *12*, 425–430.
[36] K. Müller, R. Engesser, S. Schulz, T. Steinberg, P. Tomakidi, C. C. Weber, R. Ulm, J. Timmer, M. D. Zurbriggen, W. Weber, *Nucleic Acids Res.* **2013**, *41*, DOI 10.1093/nar/gkt340.
[37] F. Richter, U. S. Scheib, J. Mehlhorn, R. Schubert, J. Wietek, O. Gernetzki, P. Hegemann, T. Mathes, A. Möglich, *Photochem. Photobiol. Sci. Off. J. Eur. Photochem. Assoc. Eur. Soc. Photobiol.* **2015**, *14*, 270–279.
[38] Á. Inglés-Prieto, E. Reichhart, M. K. Muellner, M. Nowak, S. M. B. Nijman, M. Grusch, H.

Janovjak, *Nat. Chem. Biol.* **2015**, *11*, 952–954.
[39] E. J. Olson, L. A. Hartsough, B. P. Landry, R. Shroff, J. J. Tabor, *Nat. Methods* **2014**, *11*, 449–455.
[40] V. Agus, H. Janovjak, *Curr. Opin. Biotechnol.* **2017**, *48*, 8–14.
[41] A. M. Chagas, L. L. Prieto-Godino, A. B. Arrenberg, T. Baden, *PLOS Biol.* **2017**, *15*, e2002702.
[42] A. Levskaya, A. A. Chevalier, J. J. Tabor, Z. B. Simpson, L. A. Lavery, M. Levy, E. A. Davidson, A. Scouras, A. D. Ellington, E. M. Marcotte, et al., *Nature* **2005**, *438*, 441–442.
[43] J. J. Tabor, A. Levskaya, C. A. Voigt, *J. Mol. Biol.* **2011**, *405*, 315–324.
[44] X. Chen, R. Liu, Z. Ma, X. Xu, H. Zhang, J. Xu, Q. Ouyang, Y. Yang, *Cell Res.* **2016**, *26*, 854–857.
[45] T. Han, Q. Chen, H. Liu, *ACS Synth. Biol.* **2017**, *6*, 357–366.
[46] A. Baumschlager, S. K. Aoki, M. Khammash, *ACS Synth. Biol.* **2017**, *6*, 2157–2167.
[47] P. Ramakrishnan, J. J. Tabor, *ACS Synth. Biol.* **2016**, *5*, 733–740.
[48] M. S. Magaraci, J. G. Bermudez, D. Yogish, D. H. Pak, V. Mollov, J. Tycko, D. Issadore, S. G. Mannickarottu, B. Y. Chow, *ACS Synth. Biol.* **2016**, *5*, 781–785.
[49] M. S. Magaraci, A. Veerakumar, P. Qiao, A. Amurthur, J. Y. Lee, J. S. Miller, M. Goulian, C. A. Sarkar, *ACS Synth. Biol.* **2014**, DOI 10.1021/sb400174s.
[50] L. B. Motta-Mena, A. Reade, M. J. Mallory, S. Glantz, O. D. Weiner, K. W. Lynch, K. H. Gardner, *Nat. Chem. Biol.* **2014**, *10*, 196–202.
[51] X. Wang, X. Chen, Y. Yang, *Nat. Methods* **2012**, *9*, 266–269.
[52] G. P. Pathak, J. I. Spiltoir, C. Höglund, L. R. Polstein, S. Heine-Koskinen, C. A. Gersbach, J. Rossi, C. L. Tucker, *Nucleic Acids Res.* **2017**, *in press*, DOI 10.1093/nar/gkx260.
[53] J. E. Toettcher, D. Gong, W. A. Lim, O. D. Weiner, *Nat. Methods* **2011**, *8*, 837–839.
[54] A. A. Kaberniuk, A. A. Shemetov, V. V Verkhusha, *Nat. Methods* **2016**, *13*, 591–597.
[55] A.-M. Reimers, H. Knoop, A. Bockmayr, R. Steuer, *Proc. Natl. Acad. Sci. U. S. A.* **2017**, DOI 10.1073/pnas.1617508114.
[56] T. Mathes, C. Vogl, J. Stolz, P. Hegemann, *J. Mol. Biol.* **2009**, *385*, 1511–1518.

Figures

Figure 1. A) The plasmids pDusk and pDawn employ the light-responsive two-component system (TCS) YF1/*Bj*FixJ to mediate light-repressed and light-activated gene expression, respectively[25]. The plasmid pDawn is derived from pDusk via insertion of a gene-inversion cassette based on the phage λ repressor cI. B) Kinetic model of YF1/*Bj*FixJ TCS as implemented on the pDusk plasmid. Y_{DD}, Y_{LD}, Y_{LD} and Y_{LL} denote the dimeric YF1 receptor with its two LOV domains in the states specified by the subscript, i.e. D and L for the dark-adapted and light-adapted state, respectively. YF1 is photoactivated in a forward reaction determined by the rate constant k_I and the intensity of applied blue light I; k_R denotes the dark-recovery rate constant. Note that the two LOV photosensors transition between their respective states D and L independently from another as previously shown[23]. The fully dark-adapted species Y_{DD} catalyzes the phosphorylation of the response regulator *Bj*FixJ with rate constant k_K. In its partially or fully light-adapted state (Y_{LD}, Y_{LD} and Y_{LL}) YF1 acts as a phosphatase on phospho-FixJ and catalyzes the hydrolysis of the phosphoryl group with rate constant k_P; the rate of spontaneous hydrolysis is given by k_H. Once phosphorylated, *Bj*FixJ binds as a homodimer to its cognate FixK2 promoter, governed by the affinity constant K_J, to activate transcription with a rate constant k_T. C) The

numerical solution of the kinetic scheme in panel A illustrates the time evolution of the different molecular species (Y_{DD}, black; Y_{LD}/Y_{DL}, orange; Y_{LL}, blue; phospho-*Bj*FixJ, grey) during regimes of alternating illumination (blue shading) and darkness. D) Schematic of the Arduino-based programmable LED matrix. (1) Spring clip, (2) O_2-permeable sealing film, (3) black-wall, transparent-bottom 96-well microtiter plate, (4) bacterial culture, (5) adapter, (6) eight-by-eight LED array, (7) mounting plate.

Figure 2. Control of gene expression from pDusk (upper row) and pDawn (lower row) with illumination of varying intensity and pulse frequency. A) (left column) Steady-state expression of *Ds*Red from the pDusk and pDawn plasmids while incubating under pulsed illumination. Samples were alternately illuminated for 30 s at 470 nm at variable intensities, followed by incubation in the dark for variable time periods. The contour plots show the dependence of reporter-gene expression on the duration of the dark period (*x* axis) and intensity of applied pulsed light (*y* axis). The fluorescence data are shown as color code and represent averages of three replicates ± s.d., normalized to the maximum fluorescence value of either pDusk-*Ds*Red or pDawn-*Ds*Red. (right column) The experimental data were globally fitted to the numerical solution of the kinetic scheme depicted in Fig. 1B. B) Overall, the *Ds*Red reporter-gene expression for the pDawn plasmid increased hyperbolically with time-averaged light dose. C) However, at low average light doses between 0 and 2.5 µW cm^{-2}, the system output greatly varied with the pulse frequency of light. In particular, higher gene expression output was systematically obtained if the light dose was distributed across several pulses of lower intensity, rather than a single pulse of high intensity. The colored symbols denote data obtained for different intensities of applied light (yellow circles, 2 µW cm^{-2}, orange diamonds, 8 µW cm^{-2}, green squares, 55 µW cm^{-2}, blue triangles, 78 µW cm^{-2}, and red pentagons, 105 µW cm^{-2}).

Figure 3. Modulating the intensity/pulse frequency response of light-regulated gene expression. A) Introduction of the residue exchanges V28T (blue) and V28I (red) caused acceleration or deceleration, respectively, of the YF1 dark-recovery kinetics (k_R). Absorption data were recorded at 37°C following saturating illumination of purified proteins with blue light and were fitted to single-exponential functions. The bottom panel shows the very slow recovery kinetics for the V28I variant. B) *Ds*Red expression in the pDusk and pDawn variants YF1, V28T and V28T as a function of pulse frequency and intensity of blue light. The contour plots show *Ds*Red reporter-gene expression normalized to the maxima obtained for pDusk-*Ds*Red or pDawn-*Ds*Red, respectively, as a function of light intensity and duration of dark period. To better visualize data at short dark periods, the *x* axis was split at 500 s, as indicated by the vertical white line. Fluorescence values are shown as color code and represent

averages of three replicates ± s.d. C) Individual control of several light-dependent gene-expression systems by varying intensity and frequency of pulsed illumination. *E. coli* cultures harboring the YF1 (black), V28T (blue) and V28I (red) variants of pDawn-*Ds*Red were incubated under different lighting protocols as indicated. Resultant reporter-gene expression was determined as the average of three biological replicates ± s.d. and normalized as before. Bottom row shows photographs of corresponding cultures grown in microtiter plates.

Figure 4. Intensity/pulse frequency response of variant gene-expression systems to intermittent illumination. In both the pDusk-*Ds*Red and pDawn-DsRed contexts, the YF1 variants D21V and H22P showed inverted gene expression output relative to the original YF1 system. Fluorescence data represent the average ± s.d. of three biological replicates, are normalized to the maximum output of the pDusk-*Ds*Red and pDawn-*Ds*Red systems, respectively, and are shown as color code. Responsiveness to light was retained in pDusk-*Ds*Red and pDawn-*Ds*Red variants despite replacement of the adduct-forming cysteine residue 62 in the YF1 photoreceptor by alanine, as most clearly seen for the pDusk-*Ds*Red H22P:C62A variant that fully conserved the light-dependent regulation of gene expression.

Table of contents caption.

The pulse frequency of intermittent light complements light quantity and quality as an additional input variable for controlling system output in optogenetics and photobiology. Pulsed illumination of a single color suffices for sequentially triggering expression of several genes.

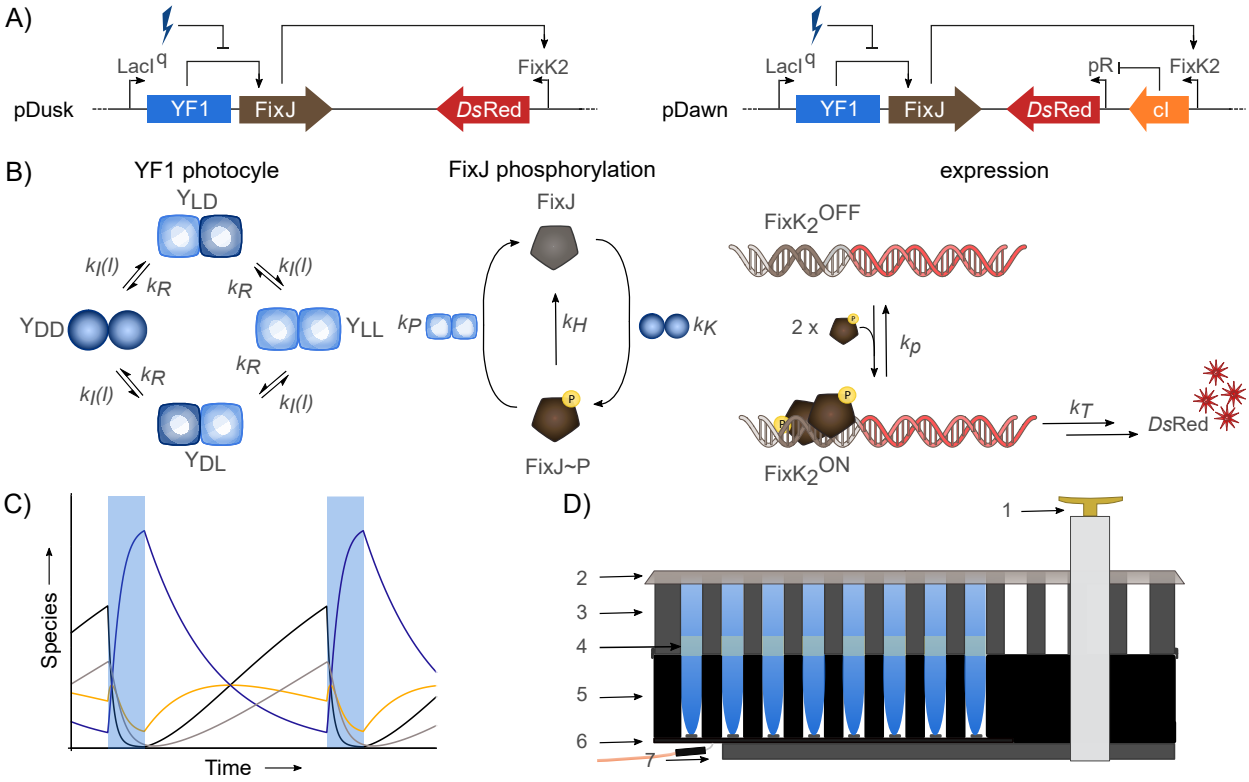
A)
pDusk
LacI^q
YF1
FixJ
DsRed
FixK2
pDawn
pR
cI
B)
YF1 photocyle
FixJ phosphorylation
expression
YLD
YDD
YLL
YDL
kI(l)
kR
kP
kH
kK
FixJ
FixJ~P
FixK2OFF
FixK2ON
2 x
kp
kT
DsRed
C)
Species
Time
D)
1
2
3
4
5
6
7

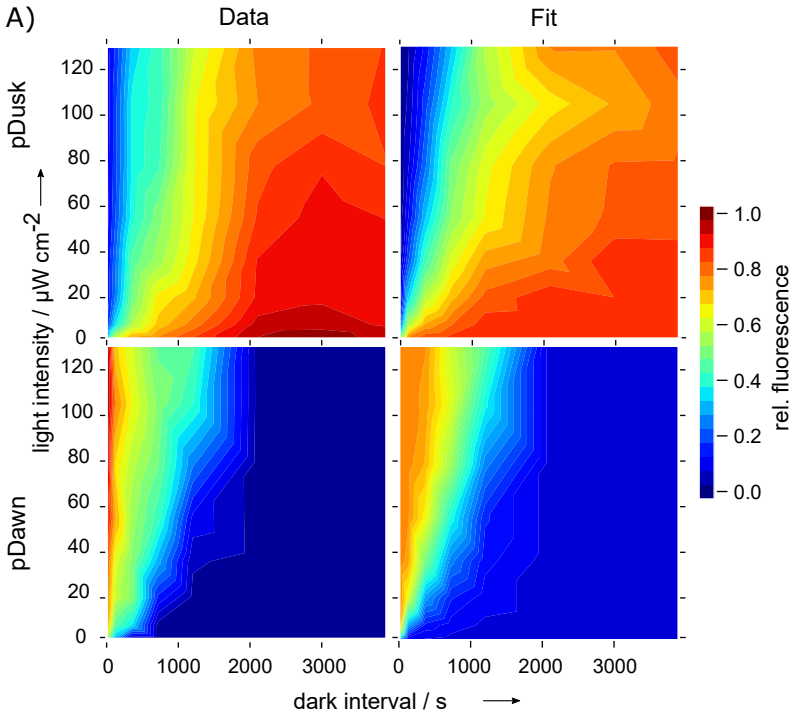
A)
Data
Fit
pDusk
pDawn
light intensity / µW cm-2
dark interval / s
rel. fluorescence
0
20
40
60
80
100
120
0
1000
2000
3000
0.0
0.2
0.4
0.6
0.8
1.0

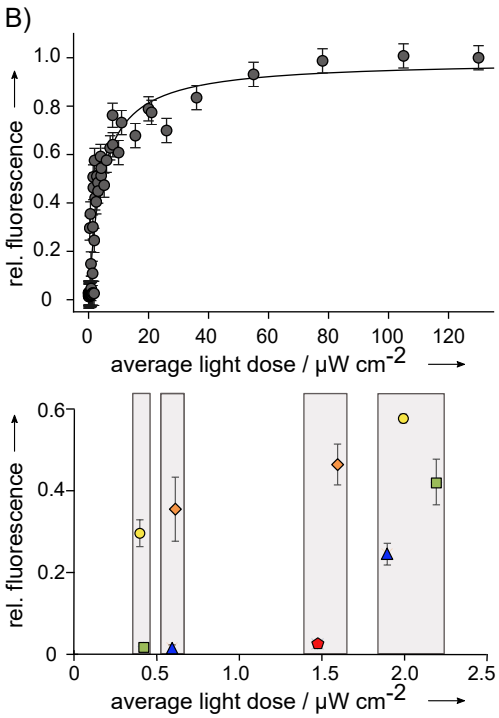
B)
rel. fluorescence
average light dose / µW cm-2
0
0.2
0.4
0.6
0.8
1.0
0
20
40
60
80
100
120
0.5
1.0
1.5
2.0
2.5

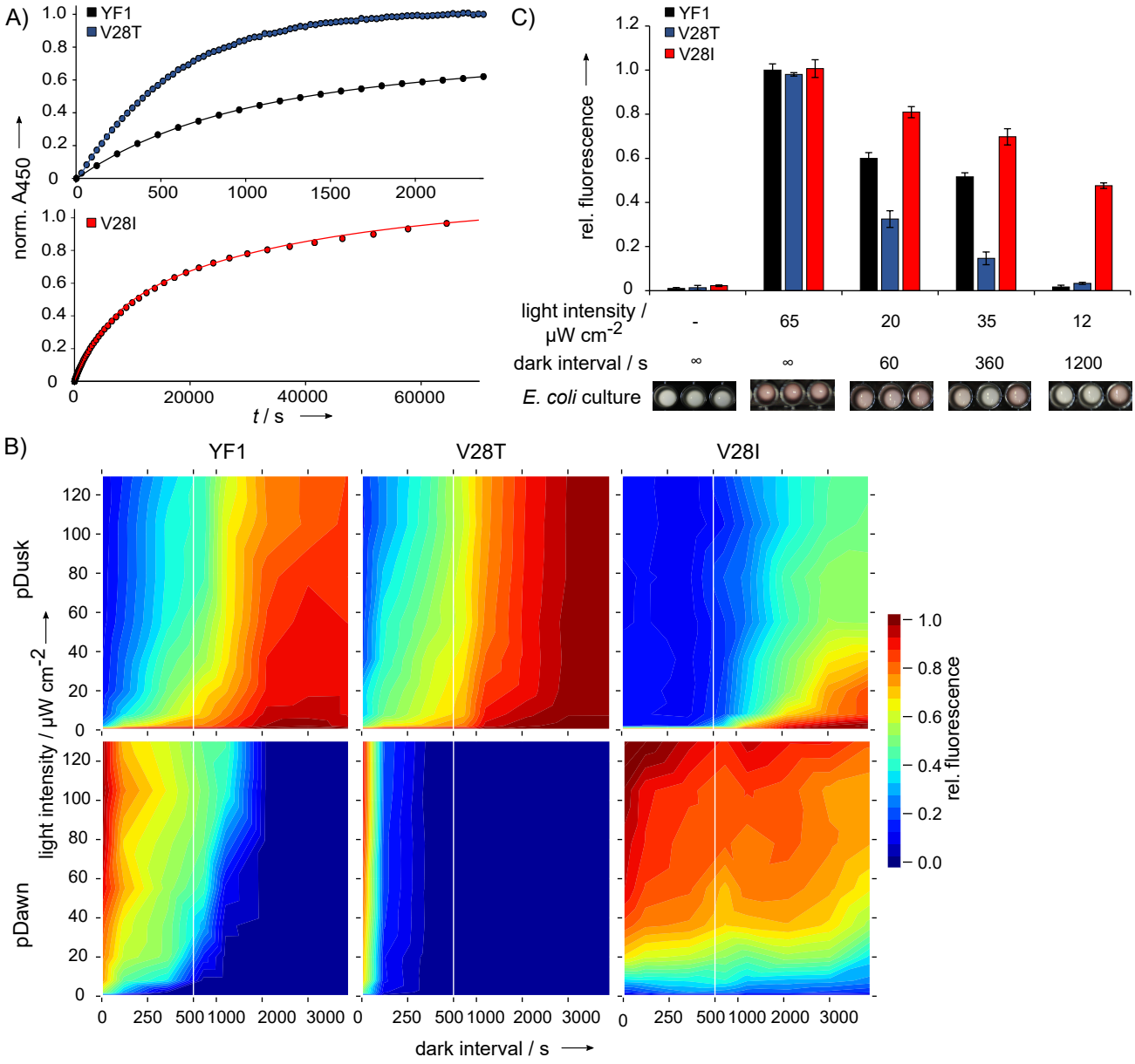
A)
YF1
V28T
V28I
norm. A450
t / s
C)
rel. fluorescence
light intensity / µW cm-2
dark interval / s
E. coli culture
B)
YF1
V28T
V28I
pDusk
pDawn
light intensity / µW cm-2
dark interval / s
rel. fluorescence

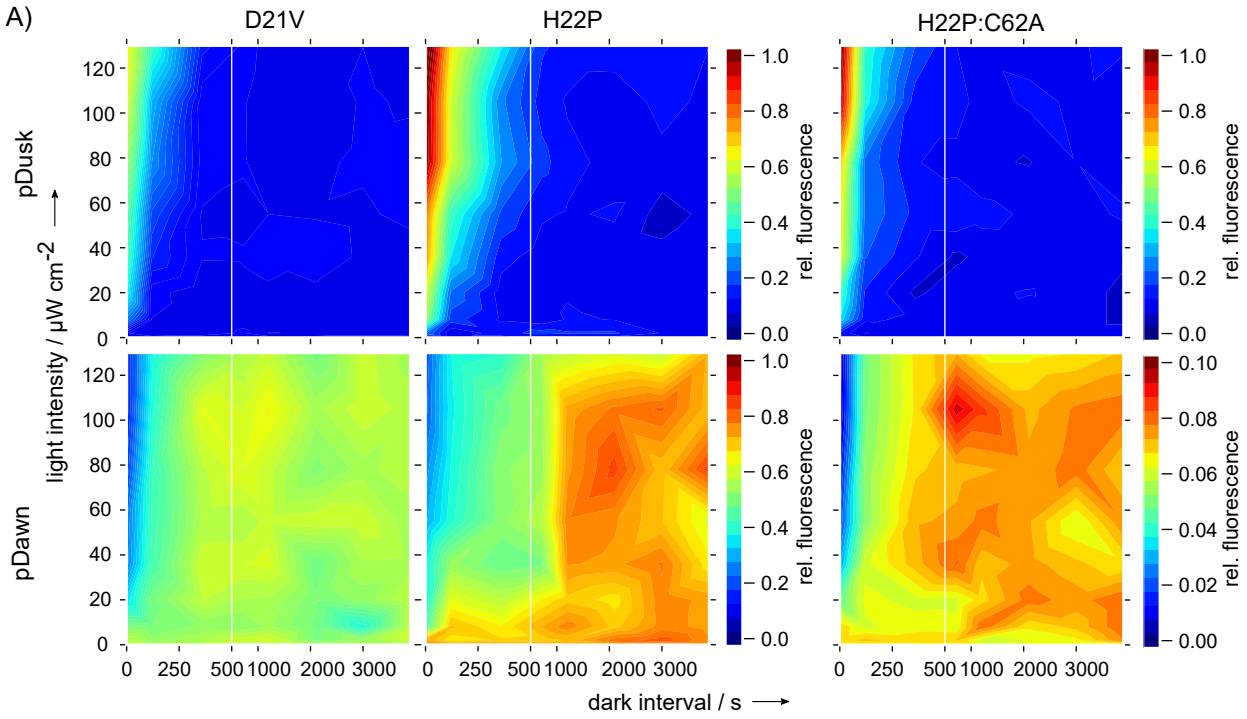
A)
D21V
H22P
H22P:C62A
pDusk
pDawn
light intensity / µW cm-2
dark interval / s
rel. fluorescence
0
20
40
60
80
100
120
0
250
500
1000
2000
3000
0.0
0.2
0.4
0.6
0.8
1.0
0.00
0.02
0.04
0.06
0.08
0.10

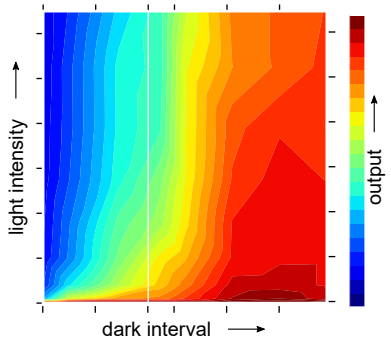
light intensity
dark interval
output